

Effects of correlated errors on the Quantum Approximate Optimization Algorithm

Joris Kattemölle and Guido Burkard

Department of Physics, University of Konstanz, D-78457 Konstanz, Germany

The Quantum Approximate Optimization Algorithm (QAOA) has the potential of providing a useful quantum advantage on Noisy Intermediate-Scale Quantum (NISQ) devices. The effects of uncorrelated noise on variational quantum algorithms such as QAOA has been studied intensively. Recent experimental results, however, show that the errors impacting NISQ devices are significantly correlated. We introduce a model for both spatially and temporally (non-Markovian) correlated errors based on classical environmental fluctuators. The model allows for the independent variation of the marginalized spacetime-local error rates and the correlation strength. Using this model, we study the effects of correlated stochastic noise on QAOA. We find evidence that the performance of QAOA improves as the correlation time or correlation length of the noise is increased at fixed local error rates. This shows that noise correlations in itself need not be detrimental for NISQ algorithms such as QAOA.

I. INTRODUCTION

Quantum computers hold the promise of outperforming classical computers on tasks such as the simulation of quantum mechanical systems [1, 2], factoring [3], unstructured database search [4], and solving linear systems of equations [5]. However, it shows to be much harder to shield qubits, the fundamental building blocks of quantum computers, from environmental noise than it is to shield classical bits [6], leading to errors in quantum computations. These errors can be detected and corrected, provided that noise rates remain below a certain threshold, as is proven by the threshold theorem for fault-tolerant quantum computation [7–10]. The theorem holds in the presence of spatially and temporally correlated errors [10–14], albeit possibly at an increased overhead in quantum resources. The quantum overhead required for fault-tolerant quantum computation is currently prohibitively large.

Nevertheless, the current, pre-error-corrected Noisy Intermediate-Scale Quantum (NISQ) [15] computers can already outperform classical computers on some tasks, and have hence shown what is called a quantum advantage [16, 17]. The tasks for which a quantum advantage has been demonstrated are artificial and have no known applications. Thus, the next milestone in the field will be the demonstration of a *useful* quantum advantage.

The hybrid quantum-classical variational quantum algorithms (VQAs) form a large set of algorithms with the potential of showing a useful quantum advantage on NISQ devices [18]. In these algorithms, a parameterized quantum state, called the ansatz, is prepared using a parameterized quantum circuit. Sequentially, the expectation value of some observable (which depends on the specific VQA) is estimated by repeated preparation and measurement of the ansatz. The parameters and resulting expectation value are fed into a classical optimization algorithm, which in turn suggest new parameters. By repeating the above steps, the optimized heuristically seeks parameters that optimize the cost function landscape. The VQA returns the optimal value of the cost function

landscape and the parameters at which it was attained.

The Quantum Approximate Optimization Algorithm (QAOA) [19] is a VQA designed to (approximately) solve instances from a large set of optimization problems [20], including problems of practical relevance, such as portfolio optimization [21] and correlation clustering [22]. The cost function of the optimization problem is first mapped to an Ising-type Hamiltonian whose ground state corresponds to the optimal solution of the optimization problem. This Hamiltonian is the observable being measured during the optimization loop. In the context of QAOA, the expectation value of the Hamiltonian, as a function of the variational parameters, is called the cost function landscape. Thus, QAOA seeks for approximate ground states of the Hamiltonian by optimizing the cost function landscape, and thereby finds approximate solutions to the optimization problem.

A common figure of merit for QAOA is the approx-

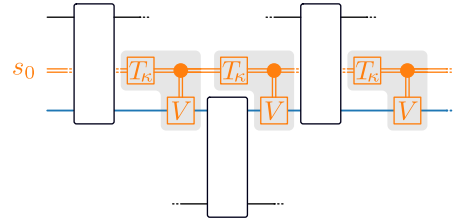


Figure 1. The temporal fluctuator model. Every qubit (blue, only one qubit fully shown) interacts with an independent classical binary fluctuator in the bath (orange, only one fluctuator shown) after every gate time. The fluctuator is initially excited with probability p , as described by the classical ensemble s_0 . The operation T_κ resets the fluctuator to s_0 with probability $1 - \kappa$. A unitary V is applied to the qubit if and only if the fluctuator is excited, leading to a model for temporally correlated errors with tunable correlation time $0 \leq \tau = -1/\log \kappa < \infty$. For a circuit of depth m , acting on n qubits, the full temporal fluctuator model is obtained by repeating the shaded area m times, and the entire arising structure n times. Empty rectangles represent generic (not necessarily two-qubit) gates. At the end of the circuit, the fluctuator is discarded (not shown).

imation ratio (AR), defined as the ratio of the expectation value of the Hamiltonian and the global optimal value of the classical cost function. Along the lines of [23], to evaluate the effects of noise, a ‘noise-unaware AR’ can be defined. The noise-unaware AR is obtained by first running QAOA in classical emulations with all noise turned off. The resulting optimal parameters are sequentially used to compute the expectation value of the Hamiltonian while the noise turned on. Thus, the resulting noise-unaware AR is the AR that would be obtained if the optimal angles cannot adapt to the noise. An AR that is larger than the noise-unaware indicates that the optimal parameters adapted to the noise, and that hence QAOA would possess a form of noise adaptivity.

The behavior of VQAs such as QAOA under local errors has been studied extensively [23–31], showing that VQAs possess forms of resilience against coherent [26, 27] and incoherent [23, 28–31] errors. VQAs [28], specifically QAOA [32], are therefore thought to be ideal candidates for obtaining a useful quantum advantage.

However, recent experimental results have highlighted the ubiquity of both spatially and temporally correlated errors in NISQ devices. Sources of spatially correlated errors include crosstalk [33, 34], fluctuations of external, quasi-homogeneous magnetic fields [35], and (cosmic) radiation [36, 37]. Sources of temporally correlated errors include reflections in drive lines [38], long-lived quasi-particle excitations [36], nuclear spins [39], and interactions with microscopic binary fluctuators [40, 41]. Given the importance of VQAs, their noise resilience against local errors, and the prevalence of correlated errors, an understanding of the effects of correlated errors on VQAs is needed.

We make a first step in this direction by studying the effects of temporally correlated (non-Markovian) and spatially correlated errors on QAOA. Inspired by recent experimental results [41], we introduce a toy model for temporally correlated errors in which every qubits interacts with a single binary fluctuator (Fig. 1). The model allows for full and independent variation of the marginalized, time-local noise rate and the correlation time. Interchanging the roles of space and time, a model for spatially correlated errors is obtained (Fig. 2). Thus, we are able to treat temporally and spatially correlated errors on an equal footing. We will therefore often write ‘correlation strength’ to refer to both correlation time and correlation length.

We classically simulate the performance of QAOA under the fluctuator error models of Figs. 1 and 2 for various problem instances, error probabilities, and error correlation strengths. Our main result is the observation of an *increase* of the performance of QAOA (as measured by the AR) as a function of correlation strength at fixed spacetime-local marginalized error rates across all cases studied [42]. We analytically derive the effect of our fluctuators models on the AR to first order in the spacetime-local noise rate p . Using this linear order theory, we show the increase in AR with correlation strength is explained

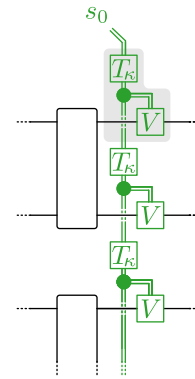


Figure 2. The spatial fluctuator model. Definitions are as in Fig. 1. As opposed to Fig. 1, the fluctuator is displayed in green, and travels through space rather than time. The error model for one circuit layer is generated by repeating the shaded area in the spatial direction n times, with n the number of qubits. The full error model is obtained by repeating the obtained structure after every gate time. The errors have correlation length $0 \leq \lambda = -1/\log \kappa < \infty$ in units of inter-qubit distance.

by a counting argument, stating that a correlated error can happen in fewer ways than an uncorrelated error. Although a single, strongly correlated error can have a stronger effect on the output state than a single error happening at a single spacetime location, in all cases we studied this does not outweigh the fact that there are simply fewer ways in which a correlated error may happen.

Additionally, we observe that the performance of QAOA degrades linearly (as measured by the AR) as a function of p around $p = 0$. Furthermore, the AR and the noise-unaware AR are essentially equal up until some critical p that depends on the fluctuator model (temporal or spatial), correlation strength and problem instance. After this critical p , the AR becomes better than the noise-unaware AR. This divergence of AR and noise-unaware AR coincides with an abrupt jump in optimal parameters that are otherwise essentially constant. This indicates that there are two competing, separated points in the cost function landscape, and that one of them overtakes the other at the critical p .

Recently, similar linear decay, noise adaptivity of optimal parameters, and critical noise rates were observed for a VQA by Fontana et al. [23]. Our results regarding these points go beyond the results of Fontana et al., firstly because we show them for QAOA, and secondly because our results also hold for correlated errors.

This paper is organized as follows. We give a more detailed introduction to QAOA in Sec. II. In Sec. III, we derive physical properties of our error model, such as correlation functions and marginalized error rates. In the same section, we derive the linear order effects of our fluctuator models on the cost function landscape. Subsequently, in Sec. IV, we describe our numerical methods,

and present and analyze our results, followed by a discussion in Sec. V.

II. QAOA

A wide class of optimization problems can be formulated using a quadratic cost function, $C(z) = \sum_{i<j}^n \omega_{ij} z_i z_j + \sum_{i=1}^n \omega_i z_i$, with $z_i \in \{-1, 1\}$ [20]. The goal is to find a $z = (z_1, \dots, z_n)$ that optimizes C globally. Depending on the specific application, the optimization is a maximization or minimization of C . The cost function can readily be mapped to a Hamiltonian,

$$H = \sum_{i<j}^n \omega_{ij} Z_i Z_j + \sum_{i=1}^n \omega_i Z_i,$$

with Z_i the Pauli-Z operator acting on qubit i . The mapping is such that $C(z) = \langle z | H | z \rangle$.

QAOA [19] bounds the optimal value of C by optimizing the cost function landscape $\tilde{C} : \mathbb{R}^{2r} \rightarrow \mathbb{R}$, with

$$\tilde{C}(\boldsymbol{\beta}, \boldsymbol{\gamma}) = \langle \boldsymbol{\beta}, \boldsymbol{\gamma} | H | \boldsymbol{\beta}, \boldsymbol{\gamma} \rangle, \quad (1)$$

by a classical heuristic optimization method of choice. Here, $|\boldsymbol{\beta}, \boldsymbol{\gamma}\rangle$ is the ansatz quantum state, depending on $2r$ parameters. It is prepared on a quantum computer by

$$|\boldsymbol{\beta}, \boldsymbol{\gamma}\rangle = \prod_{k=1}^r \mathcal{C}(\beta_k, \gamma_k) |+\rangle^{\otimes n}, \quad (2)$$

with $|+\rangle = (|0\rangle + |1\rangle)/\sqrt{2}$, and the cycle

$$\begin{aligned} \mathcal{C}(\beta_k, \gamma_k) &= \exp\left(-i\frac{\beta_k}{2} \sum_{i=1}^n X_i\right) \exp\left(-i\frac{\gamma_k}{2} H\right) \\ &= RX^{\otimes n}(\beta_k) \left[\prod_i RZ(\omega_i \gamma_k) \right] \\ &\quad \times \left[\prod_{i<j} RZZ_{ij}(\omega_{ij} \gamma_k) \right]. \end{aligned}$$

Here, $RX(\alpha) = e^{-i\alpha X/2}$, $RZ(\alpha) = e^{-i\alpha Z/2}$, and $RZZ(\alpha) = e^{-i\alpha ZZ/2}$. To obtain an estimate for \tilde{C} , the ansatz state is prepared repeatedly, each time measuring H at the end of the circuit. Since H is diagonal in the computational basis, this measurement can be performed by measurements in the computational basis and classical post-processing of the measurement outcomes.

If $\omega_i = 0$, both C and H can be identified with the same undirected weighted graph, with n nodes and adjacency matrix ω_{ij} . We will henceforth make the assumption $\omega_i = 0$. The *Sherrington-Kirkpatrick* (SK) model encompasses all fully connected problem graphs with edge weights ± 1 .

When the graph described by ω_{ij} is fully connected, every cycle of the ansatz circuit requires one two-qubit

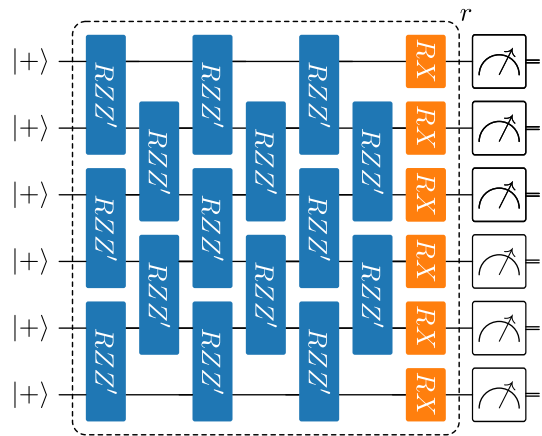


Figure 3. SWAP-network implementation of the QAOA ansatz on $n = 6$ qubits, with $RZZ' = RZZ \cdot \text{SWAP}$ and variational parameters suppressed. The ansatz cycle, marked by the dashed line, is applied to the initial state $|+\rangle^{\otimes n}$ for r times, each time with new parameters. The cost function landscape is obtained through repeated preparation, measurement and classical post-processing.

gate RZZ between every pair of qubits. To accomplish this on quantum hardware without all-to-all connectivity, SWAP-gates need to be inserted. On hardware with square-grid or line connectivity, the optimal way of doing so is by a SWAP-network [43, 44]. In the SWAP-network implementation of the ansatz circuit (Fig. 3), the order of the product of RZZ gates forms a brickwork structure, and a SWAP gate is inserted after every RZZ gate [45].

On NISQ devices, the ansatz state will be described by a mixed state $\rho(\boldsymbol{\beta}, \boldsymbol{\gamma})$. In this work, the focus is on correlated noise during the ansatz circuit, and we will therefore assume perfect estimation of \tilde{C} throughout. That is, we use

$$\tilde{C}(\boldsymbol{\beta}, \boldsymbol{\gamma}) = \text{tr}[\rho(\boldsymbol{\beta}, \boldsymbol{\gamma})H] \quad (3)$$

to compute the energy landscape in our classical emulation of QAOA (Sec. IV). From $\omega_{ij} \in \{1, -1\}$ and the periodicity of RZZ (and RZZ') with period 2π , it follows that $\mathcal{C}(\beta_k, \gamma_k)$ is invariant (up to a global phase) under $\gamma_k \mapsto \gamma_k \pm 2\pi$ for any k . As a consequence, the noiseless cost function landscape is periodic in γ_k with period 2π for any k . A similar statement holds for RX . Because of properties of the circuit ansatz and the SK Hamiltonian, much stronger symmetry relations hold, which are derived in Appendix B. In the same appendix, we prove that these symmetries are not broken by spatio-temporally correlated Pauli noise channels, which includes our fluctuator models if V is a Pauli operator.

A widely used figure of merit of optimization algorithms is the *Approximation Ratio* (AR),

$$AR = \frac{\tilde{C}(\boldsymbol{\beta}^*, \boldsymbol{\gamma}^*)}{C^*}, \quad (4)$$

with $\boldsymbol{\beta}^*, \boldsymbol{\gamma}^*$ the optimal parameters as returned by the optimization algorithm, and C^* the true, global optimum

of the cost function C . The algorithm has found the global optimum of C if and only if $AR = 1$. In a noisy implementation of QAOA, the AR that is reached is in principle *noise aware*; noise may cause the optimum of \tilde{C} to change, and the optimal parameters may adapt to this change by classical heuristic optimization.

To assess the resilience of QAOA against correlated errors, in this work we also consider the *noise unaware* AR. In classical emulation, where noise rates can be changed at will, QAOA can be run without noise, obtaining the optimal parameters β_0^*, γ_0^* . These parameters are thus unaware of the effects of noise on the cost function landscape. Putting them into the noisy circuit, we obtain $\tilde{C}(\beta_0^*, \gamma_0^*)$. Thus, we define the *noise unaware* AR as

$$AR_0 = \frac{\tilde{C}(\beta_0^*, \gamma_0^*)}{C^*}. \quad (5)$$

Using the noise unaware AR, we define the *noise adaptivity* as

$$\Delta AR = AR - AR_0. \quad (6)$$

Given that the optimum found in the noiseless case and the optimum found in the noisy case are global, we have $\Delta AR \geq 0$, where $\Delta AR \neq 0$ indicates that the optimal parameters have adapted to the noise.

A quantity similar to AR_0 was introduced in Ref. [23]. There, instead of the expectation value of the Hamiltonian, the fidelity between the ansatz state and a target state was used as the cost function. Furthermore, the optimal noise aware parameters were obtained by using the noise unaware parameters as the initial point of optimization. This led the authors of [23] to call their noise aware parameters the *reoptimized* parameters. The advantage of reoptimization is that $\Delta AR \geq 0$ is guaranteed. In the current work, we find the optimal parameters for AR and AR_0 independently to prevent any bias of the noise aware optimal parameters to points close to the noise unaware parameters. Furthermore, our data (Sec. IV) obeys $\Delta AR \geq 0$ without enforcing this property by reoptimization.

III. ERROR MODEL

The internal time evolution of a single fluctuator can be described by a binary, discrete-time and time-homogeneous Markov chain. (See e.g. Refs. [46, 47] for background information on Markov chains.) Using this formulation, we obtain the correlation time, time-local marginalized error probabilities, and the expected number of errors of the error model. Analytical first order effects of *uncorrelated* errors in the context of variational quantum algorithms were studied before in Refs. [23–25]. We extend these methods to derive the analytical first order effects of our correlated error models on QAOA.

In this section, we use terminology from the model of temporally correlated errors. Nonetheless, the results

hold for the spatial fluctuator model if the state of the fluctuator after circuit layer i is reinterpreted as the state of the fluctuator after qubit i . Thus, the correlation time becomes a correlation length.

A. Classical fluctuator

Consider a single classical binary fluctuator with ground state $(1, 0)$ and excited state $(0, 1)$. If the fluctuator is excited with probability $0 \leq p \leq 1$, its state is described by the ensemble

$$s_0 = \begin{pmatrix} 1-p \\ p \end{pmatrix}.$$

This does not represent a quantum state, but a classical ensemble equivalent to the classical mixed quantum state $\text{diag}(s_0)$. We take s_0 as the initial state of the fluctuator. Define the random variable (RV)

$$B[(1, 0)^T] = 0, \quad B[(0, 1)^T] = 1,$$

which can, e.g., be imagined as the strength of a magnetic field caused by the fluctuator at its associated qubit.

At time t (in units of gate time), the state of the fluctuator, s_t , is retained with probability $0 \leq \kappa \leq 1$, and it is reset to s_0 with probability $1 - \kappa$. After this process, the state is given by $s_{t+1} = T s_t$, with T the transition matrix,

$$T = \begin{pmatrix} \kappa + (1 - \kappa)(1 - p) & (1 - \kappa)(1 - p) \\ (1 - \kappa)p & \kappa + (1 - \kappa)p \end{pmatrix}. \quad (7)$$

To see that T describes the desired process, assume, for example, that at time t , the fluctuator is excited; $s_t = (0, 1)^T$. After it is reset with probability $1 - \kappa$, there are two ways in which it can remain excited: either the fluctuator was not reset, which happens with probability κ , or the fluctuator was reset to s_0 , but is excited merely because in the state s_0 , the fluctuator is excited with probability p . Thus, the overall probability that the fluctuator remains excited is $(0, 1)T(0, 1)^T = T_{11} = \kappa + (1 - \kappa)p$. Other entries of T follow similarly. Note T_{ba} describes the probability to transition from the state a to b (in terms of RV values).

The initial state s_0 is a steady state of T because T sends s_0 to s_0 both when the state is kept and when it is reset. (Explicit diagonalization is a simple way to check that this is the only non-trivial steady state). Thus, from an ensemble viewpoint, the Markov chain is trivial; $s_t = T^t s_0 = s_0$ for all t . Therefore, the marginalized, time-local probability to be in the excited state is p , independent of t and κ . Under the definition $B_t = B(s_t)$, it follows that $\mathbb{E}(B_t) = p$ for all t . Defining the RV $B_{\text{tot}} = \sum_{t'=0}^t B_{t'}$, it follows by the linearity of expectation values, which also holds for correlated RVs, that the expected number of times the fluctuator has been excited from $t = 0$ up to and including $t = t'$ is simply $(t + 1)p$, irrespective of κ .

The state of the fluctuator at time t is given by $s_t = T^t s_0$, where the t th matrix power of T is given by

$$T^t = \begin{pmatrix} 1 - p + p\kappa^t & 1 - p - \kappa^t + p\kappa^t \\ p - p\kappa^t & p + \kappa^t - p\kappa^t \end{pmatrix}.$$

Note that Eq. (7) is retrieved at $t = 1$. With a concise expression for T^t at hand, the correlator $\mathcal{C}(\Delta t) = \mathbb{E}(B_t B_{t+\Delta t}) - \mathbb{E}(B_t)\mathbb{E}(B_{t+\Delta t})$, which does not depend on t by time-uniformity, is computed straightforwardly, yielding

$$\mathcal{C}(\Delta t) = 4p(1-p)\kappa^{|\Delta t|}.$$

That is, correlations decay exponentially, with $1/e$ correlation time

$$\tau = -\frac{1}{\log \kappa}.$$

Thus, the correlation time increases monotonically from 0 to ∞ as κ is increased from 0 to 1.

Even though $s_t = T^t s_0 = s_0$ for all t , in the course of every physical run of a quantum circuit involving m circuit layers, a non-trivial *realization* $X \in \{(1, 0)^T, (0, 1)^T\}^{m+1}$ of fluctuator states is sampled. Equivalently, we can say that during every run, a bitstring $b \in \{0, 1\}^{m+1}$ of RV values is sampled. The realization b occurs with probability

$$p_b = [\delta_{b_0,0}(1-p) + \delta_{b_0,1}p] \prod_{t=0}^{m-1} T_{b_{t+1}b_t}. \quad (8)$$

With this expression, it can be seen with an explicit calculation that, also from the realization viewpoint, the marginalized, time-local probability that the fluctuator is excited at time t is

$$p(b_t = 1) = \sum_{b:b_t=1} p_b = p,$$

independent of t and κ .

B. Effect on expectation values

Directly after the fluctuator has transitioned from b_{t-1} to b_t , the unitary V is applied to the associated qubit, conditioned on the state of the fluctuator. The transition and the controlled unitary do not change the reduced state of the fluctuator, but correlations are built up by the controlled unitary nevertheless. At the end of the circuit, all fluctuators are traced out. Let U_1, \dots, U_m be the layers of a quantum circuit and let ρ be its initial state. In QAOA, these layers will depend on the variational parameters β, γ , but in this section, their notation is mostly suppressed. The effect of a single fluctuator f in the temporal fluctuator model, at the end of the circuit and after tracing out the fluctuator, is described by

the noisy circuit

$$\tilde{U}_f(\rho) = \sum_{b^f} p_{b^f} \tilde{U}_{b^f} \rho_0 \tilde{U}_{b^f}^\dagger, \quad \tilde{U}_{b^f} = \prod_{t=m}^1 V_{b_t^f} U_t,$$

with p_{b^f} as in Eq. (8) (after substituting $b \rightarrow b^f$), \tilde{U}_{b^f} the circuit in case of noise realization b^f , and $\rho_0 = |+\rangle\langle+|$ the initial state. Here, $V_{b_t^f}$ is an operator acting just after time t and just before the gates U_{t+1} on the qubit associated with f , with $V_0 \equiv \mathbb{1}$, $V_1 \equiv V$.

Because the n realization probability distributions $\{p_{b^f}\}_f$ are independent and identically distributed, their combined effect on the output state is

$$\tilde{U}(\rho) = \sum_b p_b \tilde{U}_b \rho_0 \tilde{U}_b^\dagger, \quad (9)$$

with

$$p_b = \prod_{f=1}^n (p_{b^f}), \quad \tilde{U}_b = \prod_{t=m}^1 (V_{b_t} U_t), \quad V_{b_t} = \prod_{f=n}^1 (V_{b_t^f}). \quad (10)$$

In the spatial fluctuator model, we again have Eq. (9), but with

$$p_b = \prod_{t=1}^m (p_{b^t}), \quad \tilde{U}_b = \prod_{t=1}^m (V_{b^t} U_t), \quad V_{b^t} = \prod_{q=1}^n (V_{b_q^t}).$$

In the spatial model, the different fluctuators carry the label t . Fluctuator t transitions from the state b_q^t to b_{q+1}^t as it ‘moves’ from qubit q to $q+1$.

Returning to the temporal fluctuator model, we define the susceptibility of the cost function to noise at optimal variational parameters (as found by QAOA) as $\chi = (d\langle H \rangle / dp)_{p=0}$, with $\text{tr}[\rho(\beta_0^*, \gamma_0^*)H] \equiv \langle H \rangle$ for short. Using χ , we may write the first order approximation to the AR, which we call the *linearized AR*, as

$$AR^{\text{lin}}(p) = AR(0) + p \frac{\chi}{C_*}, \quad (11)$$

where we have by Eq. (9) that

$$\chi = \sum_b \left. \frac{dp_b}{dp} \right|_{p=0} \text{tr} \left(\tilde{U}_b \rho_0 \tilde{U}_b^\dagger H \right). \quad (12)$$

Since p_b [Eq. (8)] is some explicit polynomial in p and κ , it is clear that the derivative with respect to p at $p=0$ can be computed analytically. The resulting expression for χ is derived in Appendix A. The expression becomes especially clear in the limits of no correlation ($\kappa=0$) and full correlation ($\kappa=1$),

$$\chi_\kappa^{(a)} = |\mathcal{B}_{1+a\delta_{\kappa 1}}| \{ \langle H \rangle^{(1+a\delta_{\kappa 1})} - \langle H \rangle_0 \}, \quad (13)$$

where $a = m$ for fully temporally correlated errors, and $a = n$ for fully spatially correlated errors. Here, \mathcal{B}_ℓ is the set of realizations b where exactly one fluctuator has exactly one chain of ℓ subsequent excitations (no other

excitations in any fluctuator present), $\langle H \rangle^{(\ell)}$ is the expectation value of H given realization b , averaged over all $b \in \mathcal{B}_\ell$, and $\langle H \rangle_{\mathbf{0}}$ is the expectation value of H in the noiseless case.

For fully temporally correlated errors, we have the prefactor $|\mathcal{B}_{1+m}| = n$, for fully spatially correlated errors, $|\mathcal{B}_{1+n}| = m$, and for fully uncorrelated errors $|\mathcal{B}_1| = n(m+1)$. So, roughly speaking, there are two effects that determine whether we should expect $\chi_0 > \chi_1$ or $\chi_0 < \chi_1$. On the one hand, one expects that (i), on average, the detrimental effect of a fully correlated error, consisting of m consecutive errors (n adjacent errors in the case of spatially correlated errors) on $\langle H \rangle$ is larger than the detrimental effect of 1 error on $\langle H \rangle$. That is, one expects $(\langle H \rangle^{(m+1)} - \langle H \rangle_{\mathbf{0}}) > (\langle H \rangle^{(1)} - \langle H \rangle_{\mathbf{0}})$ and $(\langle H \rangle^{(n+1)} - \langle H \rangle_{\mathbf{0}}) > (\langle H \rangle^{(1)} - \langle H \rangle_{\mathbf{0}})$. On the other hand, (ii) there are fewer ways in which a fully correlated error can happen: a fully temporally correlated error can happen in n different ways and a fully spatially correlated error can happen in m different ways, whereas a single uncorrelated error can happen in nm ways. [The latter still leads to a prefactor of $|\mathcal{B}_1| = n(m+1)$ because of the way $\langle H \rangle^{(1)}$ is defined.] If the effect (ii) is dominant, we expect that for narrow circuits ($n \ll m$), the AR is highest with fully temporally correlated errors, followed by the AR with fully spatially correlated errors, followed by the fully uncorrelated errors.

IV. NUMERICAL METHODS AND RESULTS

In this section, we present numerical data on the SWAP-network implementation of QAOA (Fig. 3) under the influence of the temporal and spatial fluctuator models for 16 random instances of the SK problem (i.e. problems with edge weights $\omega_{ij} \in \{+1, -1\}$, see Sec. II). As the error operator V , we choose the bit-phaseflip error or Pauli- Y error. This choice is motivated by the fact that Y is the only non-trivial single-qubit Pauli operator that commutes with neither RZZ' nor RX . To exclude the possibility that an increase in AR as a function of κ is due to $Y^2 = \mathbb{1}$, which may occur, for example, due to Y -operators being inserted at $t = 1$ and $t = 2$ on the first qubit, we include an interaction between the fluctuator and its associated qubit only after the qubit was acted on by a RZZ' or RZ gate.

Simulations were performed for $n = 6$ qubits, $r = 3$ cycles (leading to $m = 21$ circuit layers), and various values of p and κ . For each combination of SK instance, type of fluctuator model, p and κ , a basin-hopping routine [48] was run 32 times to heuristically optimize \tilde{C} . The meta-parameters of the routine were the default values as per SciPy [49], but with 4 iterations, and all initial parameters β, γ chosen at random in the interval $[-0.5 \cdot 10^{-3}, 0.5 \cdot 10^{-3}]$. The mixed state ρ' at the end of the quantum circuit was obtained by full density-matrix simulation of all qubits and fluctuators, tracing out all fluctuators before computing the cost function

$\tilde{C} = \text{tr}(\rho'H)$ (variational parameters suppressed). With the full density matrix at hand, the computation of the cost function at given p, κ and variational parameters is free of shot noise and thus essentially exact. The simulator itself was obtained by extending the simulator used in Ref. [50] with the functionality of memory-efficient density-matrix simulation of mixed quantum-classical registers. All code used to generate the results in this work, including the code of the simulator, will be made freely available online.

We find qualitatively equal results for all 16 random problem instances. In this section, the results for one typical problem instance are treated quantitatively. We can gather the edge weights of an SK problem instance into a bitstring by $\omega = \prod_{i=1}^{n-1} \prod_{j=i+1}^n \omega_{ij}$. In this notation, the typical instance we consider here reads

$$\omega = ++-++-+-+-----+.$$

This instance has four degenerate global minima. Two of them are related to the other two by the symmetry $C(z) = C(\bar{z})$, with \bar{z} the bitwise negation of the bitstring z . Further details on the typical instance, its typicality, and the other 15 random instances are found in the Supplementary Material (SM) [51].

Figure 4 shows the AR as a function of p at fixed $\kappa \in \{0, 1\}$ obtained under the temporal and spatial fluctuator models. Increasing p away from 0, we observe a linear decrease of the AR, with excellent agreement between the AR, the noise unaware AR and the linearized AR. In this sense, no ‘robustness’ of QAOA against errors of the three types is observed around $p = 0$.

Out of the three types of correlation, the AR is highest for fully temporally correlated noise. Second in AR comes the fully spatially correlated noise, followed by the AR for fully uncorrelated noise. This shows that, for the instances under our study, in the extreme cases $\kappa = 0$ $\kappa = 1$, the reduction of the effects of correlated errors due to the lesser ways in which they may act, as compared to uncorrelated errors (effect ‘ii’ in Sec. III B), is dominant for small p . The order of the ARs remains unchanged for all p considered, indicating that the same effect may play a role for all p [52].

For uncorrelated noise, a sudden increase of divergence between the AR and the noise unaware AR is observed at $p_{\text{crit}} = (3.9 \pm 0.1) \times 10^{-3}$. This sudden increase of divergence coincides with an abrupt jump in the otherwise slowly varying optimal parameters [see SM]. This shows that, as p is increased away from 0, initially no other local minimum of the cost function becomes available and that the location of the initial minimum is approximately constant. For $p > p_{\text{crit}}^{\text{uncor}}$, for the first time, a remote lower local minimum becomes available. This new local minimum remains the lowest local minimum as found by QAOA until $p = 0.015 \pm 0.005$. Similar first critical points, not visible in the plot because of the scale, occur at $p_{\text{crit}}^{\text{temp}} = 0.077 \pm 0.001$ for fully temporally correlated noise, and at $p_{\text{crit}}^{\text{spat}} = 0.013 \pm 0.001$ for fully spatially correlated noise.

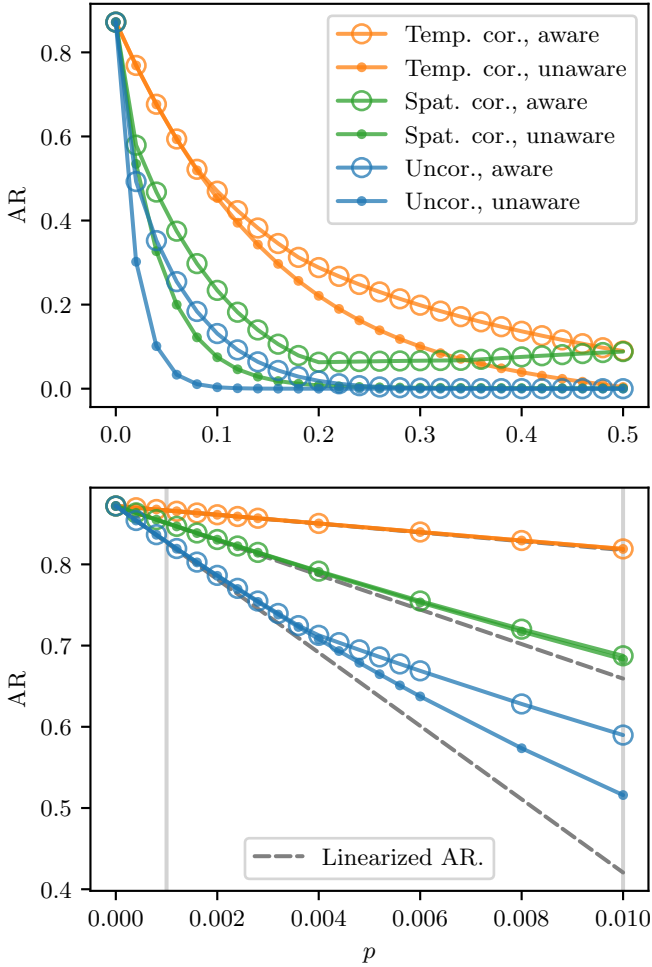


Figure 4. The approximation ratio (AR), obtained by the noisy SWAP-network implementation of QAOA for $0 \leq p \leq 0.5$ (top) and $0 \leq p \leq 0.01$ (bottom) at fixed κ . Results are shown for fully temporally correlated errors (orange), fully spatially correlated errors (green), and fully uncorrelated errors (blue). Open circles show the noise aware AR [Eq. (4)], whereas the filled circles show the noise unaware AR [Eq. (5)]. The linearized AR [Eq. (11)], is displayed as a (dashed) gray line for visibility, irrespective of noise model and correlation strength. Light gray lines at $p \in \{0.001, 0.01\}$ are for later reference. Error bars are absent because of the use of full density-matrix simulation. For the typical instance under consideration, the expected cost function value obtained by random guessing of a solution is exactly zero. Hence, the AR in the case of random guessing is exactly zero.

An increase of the noise-aware AR is seen after $p \approx 0.2$. This effect may arise because the noise creates a mixture of states, some of which may have a favorable cost. Then, increasing the noise rate may in some cases lead to an increase in AR. This effect is perhaps best illustrated by a simple example. Consider a trivial version of QAOA, with a single qubit in the initial state $|+\rangle$, no variational circuit, and Hamiltonian $H = Z$, under the effect of the error channel $\rho \mapsto (1-p)\rho + RY(\pi/2)\rho RY^\dagger(\pi/2)$. Then,

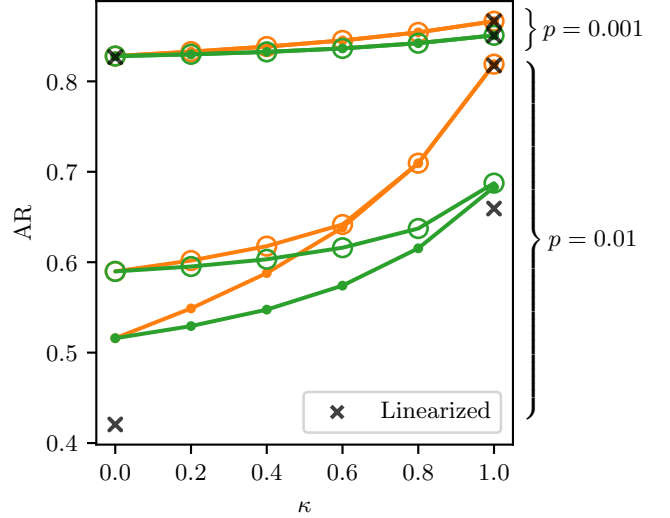


Figure 5. The approximation ratio (AR) as a function of κ , at fixed $p = 0.001$ (upper lines and crosses) and $p = 0.01$ (lower lines and crosses). The values for p correspond to the vertical lines in Fig. 4. Definitions are as in Fig. 4, except for the linearized AR, which is now displayed with crosses. At $\kappa = 0$, the temporal fluctuator model is equivalent to the spatial fluctuator model, and hence only two black crosses are shown at $\kappa = 0$, the upper one showing the linearized AR at $p = 0.001$, and the lower one showing the same at $p = 0.01$. For visibility, at $\kappa = 1$, crosses are black irrespective of type of fluctuator model and p . From top to bottom, they describe the linearized AR at $p = 0.001$ for the temporal fluctuator model and spatial fluctuator model, followed by the linearized AR for the temporal fluctuator model and spatial fluctuator model at $p = 0.01$.

with $RY(\pi/2)|+\rangle = |1\rangle$, the cost function ‘landscape’ after the error channel is $\tilde{C} = -p$. That is, in this example, $AR(p) = p$.

Figure 5 shows the AR as a function of κ at fixed $p \in \{0.001, 0.01\}$ for both fluctuator models. These values for p are chosen because typical two-qubit error rates roughly fall within the range $0.001 \lesssim p \lesssim 0.01$ [53–55]. The data suggests the noise aware AR is highest for temporally correlated errors, and that the increase in AR as a function of $\kappa > 0$ is monotonic for all fluctuator models and p considered. At $p = 0.001$, excellent agreement between the noise aware AR, noise unaware AR, and the linearized AR is shown for all $0 < \kappa < 1$ considered. At $p = 0.01, \kappa = 0$, the agreement between AR, noise unaware AR and linearized AR has been broken, as was already apparent from Fig. 4. In Fig. 5, we see how the first critical p depends on κ ; $p = 0.001$ is below p_{crit}^κ for both fluctuator models and any $0 \leq \kappa \leq 1$. In the spatial fluctuator model, $p = 0.01$ is above $p_{\text{crit}}^{\text{spat}, \kappa}$ for all $0 \leq \kappa \leq 1$. In the temporal fluctuator model, $p = 0.01$ is below $p_{\text{crit}}^{\text{temp}, \kappa}$ for κ below roughly 0.7, and above $p_{\text{crit}}^{\text{temp}, \kappa}$ for κ above roughly 0.7.

V. DISCUSSION

We studied the performance of QAOA under temporally and spatially correlated errors using a physically inspired toy error model. In the model for temporally correlated errors, every qubit interacts with one independent classical fluctuator during the course of a quantum computation. In the model for spatially correlated errors, at every gate time, all qubits interact with a single fluctuator that is reset before the next gate time. As the fluctuator moves through time (temporal model) or space (spatial model), it undergoes an internal time evolution described by a Markov process. Using the Markov formulation, we showed that the spacetime-local marginalized error rate p is independent of the correlation strength of the Markov chain, and how the latter can be varied from zero to infinity.

We showed that, to first order in the local noise rate p , the effect of the fluctuator error models on QAOA's cost function landscape has two competing factors. On the one hand, (i) the detrimental effect of a single correlated error may be worse than the effect of a single uncorrelated error, but on the other, (ii) there are far fewer ways in which a correlated error may act. For example, a fully temporally correlated error (that is, an error operation V is inserted after every gate time) during a circuit acting on n qubits can happen in n ways, a fully spatially correlated error (i.e. an error operation V is inserted at every qubit) during a circuit of depth m can happen in only m ways, whereas a fully uncorrelated error (i.e. a single error operation V is inserted anywhere in the circuit) can happen in nm ways.

We numerically emulated QAOA for 16 random Sherrington-Kirkpatrick problem instances on 6 qubits. For all instances, we observed an increase in the performance of QAOA with correlation strength at all p , indi-

cating that effect (ii) is dominant [56]. Furthermore, in all instances and at all correlation strengths, we observed the existence of critical local noise rates after which the noise-aware approximation ratio is higher than the noise-unaware approximation ratio. This shows QAOA can in some cases adapt to the effects of uncorrelated and correlated errors given that noise rates are *above* a threshold. It remains an open question how this threshold behaves as the number of qubits is increased to numbers required for a practical quantum advantage. The noise resilience of QAOA may be seriously limited if the noise adaptivity threshold increases with n .

Our work does not show that correlated errors are beneficial to QAOA; adding correlated errors *on top* of local errors will almost certainly result in reduction in the performance of QAOA. What our work indicates is that it is not correlation in itself that has a negative effect on QAOA. To improve current hardware to the point that it can demonstrate a useful quantum advantage, a reduction of both uncorrelated and correlated errors remains necessary.

Lines for future work include the study of the generality of our results. It is a priori not clear if similar effects hold in more general models of temporally and spatially correlated noise, or if they hold for other VQAs. If they do, the experimental requirements on noise correlation strengths may not be as stringent as previously thought, bringing a useful quantum advantage within closer reach.

ACKNOWLEDGMENTS

We acknowledge funding from the Competence Center Quantum Computing Baden-Württemberg, under the project QORA. Computations were carried out on the Scientific Compute Cluster of the University of Konstanz (SCCKN).

-
- [1] R. P. Feynman, *International Journal of Theoretical Physics* **21**, 467 (1982).
 - [2] S. Lloyd, *Science* **273**, 1073 (1996).
 - [3] P. Shor, in *Proceedings 35th Annual Symposium on Foundations of Computer Science* (IEEE Comput. Soc. Press, 1994).
 - [4] L. K. Grover, in *Proceedings of the twenty-eighth annual ACM symposium on Theory of computing - STOC '96* (ACM Press, 1996).
 - [5] A. W. Harrow, A. Hassidim, and S. Lloyd, *Physical Review Letters* **103** (2009).
 - [6] D. Suter and G. A. Álvarez, *Reviews of Modern Physics* **88** (2016).
 - [7] P. Shor, in *Proceedings of 37th Conference on Foundations of Computer Science* (IEEE Comput. Soc. Press, 1996).
 - [8] D. Aharonov and M. Ben-Or, in *Proceedings of the twenty-ninth annual ACM symposium on Theory of computing - STOC '97* (ACM Press, 1997).
 - [9] E. Knill, R. Laflamme, and W. H. Zurek, *Proceedings of the Royal Society of London. Series A: Mathematical, Physical and Engineering Sciences* **454**, 365 (1998).
 - [10] D. Aharonov and M. Ben-Or, *SIAM Journal on Computing* **38**, 1207 (2008).
 - [11] B. M. Terhal and G. Burkard, *Physical Review A* **71** (2005).
 - [12] D. Aharonov, A. Kitaev, and J. Preskill, *Physical Review Letters* **96** (2006).
 - [13] P. Aliferis, D. Gottesman, and J. Preskill, *Quantum Information and Computation* **6**, 97 (2006).
 - [14] J. Preskill, *Quantum Information and Computation* **13**, 181 (2013).
 - [15] J. Preskill, *Quantum* **2**, 79 (2018).
 - [16] F. Arute *et al.*, *Nature* **574**, 505 (2019).
 - [17] H.-S. Zhong, H. Wang, Y.-H. Deng, M.-C. Chen, L.-C. Peng, Y.-H. Luo, J. Qin, D. Wu, X. Ding, Y. Hu, *et al.*,

- Science **370**, 1460 (2020).
- [18] M. Cerezo, A. Arrasmith, R. Babbush, S. C. Benjamin, S. Endo, K. Fujii, J. R. McClean, K. Mitarai, X. Yuan, L. Cincio, *et al.*, *Nature Reviews Physics* **3**, 625 (2021).
- [19] E. Farhi, J. Goldstone, and S. Gutmann, “A quantum approximate optimization algorithm,” (2014), [arXiv:1411.4028](https://arxiv.org/abs/1411.4028).
- [20] A. Lucas, *Frontiers in Physics* **2** (2014).
- [21] M. Hodson, B. Ruck, H. Ong, D. Garvin, and S. Dulman, “Portfolio rebalancing experiments using the quantum alternating operator ansatz,” (2019), [arXiv:1911.05296](https://arxiv.org/abs/1911.05296) [quant-ph].
- [22] J. R. Weggemans, A. Urech, A. Rausch, R. Spreuw, R. Boucherie, F. Schreck, K. Schoutens, J. Minář, and F. Speelman, *Quantum* **6**, 687 (2022).
- [23] E. Fontana, N. Fitzpatrick, D. M. Ramo, R. Duncan, and I. Rungger, *Physical Review A* **104**, 022403 (2021).
- [24] C. Xue, Z.-Y. Chen, Y.-C. Wu, and G.-P. Guo, *Chinese Physics Letters* **38**, 030302 (2021).
- [25] J. Marshall, F. Wudarski, S. Hadfield, and T. Hogg, *IOF SciNotes* **1**, 025208 (2020).
- [26] J. R. McClean, J. Romero, R. Babbush, and A. Aspuru-Guzik, *New Journal of Physics* **18**, 023023 (2016).
- [27] P. J. O’Malley, R. Babbush, I. D. Kivlichan, J. Romero, J. R. McClean, R. Barends, J. Kelly, P. Roushan, A. Tranter, N. Ding, *et al.*, *Physical Review X* **6**, 031007 (2016).
- [28] J. R. McClean, M. E. Kimchi-Schwartz, J. Carter, and W. A. de Jong, *Physical Review A* **95** (2017).
- [29] J. Colless, V. Ramasesh, D. Dahlen, M. Blok, M. Kimchi-Schwartz, J. McClean, J. Carter, W. de Jong, and I. Siddiqi, *Physical Review X* **8** (2018).
- [30] L. Gentini, A. Cuccoli, S. Pirandola, P. Verrucchi, and L. Bianchi, *Physical Review A* **102** (2020).
- [31] K. Sharma, S. Khatri, M. Cerezo, and P. J. Coles, *New Journal of Physics* **22**, 043006 (2020).
- [32] E. Farhi and A. W. Harrow, “Quantum supremacy through the quantum approximate optimization algorithm,” (2016), [arXiv:1602.07674](https://arxiv.org/abs/1602.07674).
- [33] I. Heinz and G. Burkard, *Physical Review B* **104** (2021).
- [34] E. v. d. Berg, Z. K. Mineev, A. Kandala, and K. Temme, “Probabilistic error cancellation with sparse pauli-lindblad models on noisy quantum processors,” (2022).
- [35] T. Monz, P. Schindler, J. T. Barreiro, M. Chwalla, D. Nigg, W. A. Coish, M. Harlander, W. Hänsel, M. Hennrich, and R. Blatt, *Physical Review Letters* **106** (2011).
- [36] C. D. Wilen, S. Abdullah, N. Kurinsky, C. Stanford, L. Cardani, G. d’Imperio, C. Tomei, L. Faoro, L. Ioffe, C. Liu, *et al.*, *Nature* **594**, 369 (2021).
- [37] L. Cardani, F. Valenti, N. Casali, G. Catelani, T. Charpentier, M. Clemenza, I. Colantoni, A. Cruciani, G. D’Imperio, L. Gironi, L. Grünhaupt, D. Gusenkova, F. Henriques, M. Lagoi, M. Martinez, G. Pettinari, C. Rusconi, O. Sander, C. Tomei, A. V. Ustinov, M. Weber, W. Wernsdorfer, M. Vignati, S. Pirro, and I. M. Pop, *Nature Communications* **12** (2021).
- [38] M. Reed, “Entanglement and quantum error correction with superconducting qubits,” (2013).
- [39] A. V. Khaetskii, D. Loss, and L. Glazman, *Phys. Rev. Lett.* **88**, 186802 (2002).
- [40] G. Burkard, *Physical Review B* **79** (2009).
- [41] S. Schlör, J. Lisenfeld, C. Müller, A. Bilmes, A. Schneider, D. P. Pappas, A. V. Ustinov, and M. Weides, *Physical Review Letters* **123** (2019).
- [42] There are two instances where a single exception occurs, but these exceptions can be alluded to incomplete optimization, as we show in the supplementary material.
- [43] I. D. Kivlichan, J. McClean, N. Wiebe, C. Gidney, A. Aspuru-Guzik, G. K.-L. Chan, and R. Babbush, *Physical Review Letters* **120** (2018).
- [44] B. O’Gorman, W. J. Huggins, E. G. Rieffel, and K. B. Whaley, “Generalized swap networks for near-term quantum computing,” (2019).
- [45] A SWAP gate effectively swaps qubit indices. This has to be accounted for by changing the parameters in subsequent RZZ gates, which depend on the effective qubit labels the RZZ gate is acting on, accordingly. One way of implementing this is by keeping a list of qubit indices, initialized at $x = (1, 2, \dots, n)$. Every time a SWAP gate acts on qubits i and j , we set $x_i \leftrightarrow x_j$. Subsequently, every $RZZ(\omega_{ij}\gamma_k)$ has to be replaced with $RZZ(\omega_{x_i x_j}\gamma_k)$. For an even number of cycles, the output state of the SWAP-network implementation is identical to the output of the circuit in Eq. (2). For an uneven number of cycles, the effective order of the qubits is reversed, which can be easily accounted for in the classical post-processing of the measurement outcomes.
- [46] H.-P. Breuer and F. Petruccione, *The Theory of Open Quantum Systems* (Oxford University Press, 2007).
- [47] R. Serfozo, *Basics of applied stochastic processes* (Springer Science & Business Media, 2009).
- [48] D. J. Wales and J. P. K. Doye, *The Journal of Physical Chemistry A* **101**, 5111 (1997).
- [49] “Scipy 1.5.2 documentation,” (Accessed July 2022).
- [50] J. Kattemölle and J. van Wezel, “Variational quantum eigensolver for the heisenberg antiferromagnet on the kagome lattice,” (2021), [arXiv:2108.02175](https://arxiv.org/abs/2108.02175).
- [51] In the supplementary material we present all numerical data, including the details on the sampled instances. Data includes the AR and the distance of the optimal angles from the origin as a function of p .
- [52] A single exception occurs for one instance at $p \geq 0.04$. Here, the noise-aware AR in the case of fully spatially correlated errors becomes higher than the noise-aware AR in the case of fully temporally correlated errors. The noise-aware AR remains higher for correlated errors. See the SM.
- [53] C. Ballance, T. Harty, N. Linke, M. Sepiol, and D. Lucas, *Physical review letters* **117**, 060504 (2016).
- [54] X. Xue, M. Russ, N. Samkharadze, B. Undseth, A. Sammak, G. Scappucci, and L. M. Vandersypen, *Nature* **601**, 343 (2022).
- [55] M. Kjaergaard, M. E. Schwartz, J. Braumüller, P. Krantz, J. I.-J. Wang, S. Gustavsson, and W. D. Oliver, *Annual Review of Condensed Matter Physics* **11**, 369 (2020), <https://doi.org/10.1146/annurev-conmatphys-031119-050605>.
- [56] There are two instances where a single exception occurs, but these exceptions can be alluded to incomplete optimization, as we show in the SM.

Appendix A: Cost function landscape noise susceptibility

In this appendix we compute the derivative of the cost function landscape (at fixed parameters) of QAOA, as obtained with a circuit that is acted upon by our fluctuator models, to the local error probability p at $p = 0$.

Let us first consider a single fluctuator f . Denote the noise realizations of that fluctuator by the bistring b^f . Computing the derivative of Eq. (8), we find

$$\left. \frac{dp_{bf}}{dp} \right|_{p=0} = \sum_{\ell=1}^{m+1} \sum_{i=0}^{m+1-\ell} \delta_{b^f, 0^i 1^{\ell-k_{i\ell}}} (1-\kappa)^{2-\delta_{i,0}-\delta_{k_{i\ell},0}} \kappa^{\ell-1} - \delta_{b^f, \mathbf{0}} [m(1-\kappa) + 1], \quad (\text{A1})$$

with $k_{i\ell} = m+1-i-\ell$ the number of 0s that need to be appended to the bistring $0^i 1^\ell$ to make it a bitstring of length $m+1$.

Moving to n fluctuators, we have by Eq. (10) that

$$\left. \frac{dp_b}{dp} \right|_{p=0} = \sum_{f=1}^n \delta_{b^1 \dots b^{f-1}, \mathbf{0}} \left(\left. \frac{dp_{bf}}{dp} \right|_{p=0} \right) \delta_{b^{f+1} \dots b^n, \mathbf{0}}.$$

Then, with the definition $\langle H \rangle_b = \text{tr}(\tilde{U}_b \rho_0 \tilde{U}_b^\dagger H)$, we have by Eq. (12), that

$$\chi = \sum_{b,f,\ell,i} \tilde{\delta}_{b,f,\ell,i} (1-\kappa)^{2-\delta_{i,0}-\delta_{k_{i\ell},0}} \kappa^{\ell-1} \langle H \rangle_b - n[m(1-\kappa) + 1] \langle H \rangle_{\mathbf{0}},$$

with $\tilde{\delta}_{b,f,\ell,i} = \delta_{b^1 \dots b^{f-1}, \mathbf{0}} \delta_{b^f, 0^i 1^{\ell-k_{i\ell}}} \delta_{b^{f+1} \dots b^n, \mathbf{0}}$, and where the sum is over all b, i, j, f , in the ranges as described before. Note $\mathbf{0} = 00 \dots 0$ has varying dimension depending on context. We can write the previous expression for χ more schematically as

$$\chi = \sum_b \left[(1-\kappa)^{h(b)} \kappa^{\ell(b)-1} \langle H \rangle_b \right] - n[m(1-\kappa) + 1] \langle H \rangle_{\mathbf{0}},$$

where the sum is over all realizations b where exactly one fluctuator has exactly one chain of consecutive excitations (and no other excitations), $h(b) \in \{0, 1, 2\}$ is the number of transitions $0 \leftrightarrow 1$ in b , and $\ell(b) \geq 1$ is the length of the chain.

The average contribution of chains of errors of length ℓ to χ schematically reads $\langle H \rangle^{(\ell)} \equiv \frac{1}{|\mathcal{B}_\ell|} \sum_{b \in \mathcal{B}_\ell} (1-\kappa)^{h(b)} \langle H \rangle_b$, where the set \mathcal{B}_ℓ contains those realizations b where exactly one fluctuator has exactly one chain of excitations of length ℓ , and where we have absorbed the boundary effects $(1-\kappa)^{h(b)}$ into $\langle H \rangle^{(\ell)}$. With this definition, the susceptibility becomes

$$\chi = \sum_{\ell=1}^{m+1} \left(|\mathcal{B}_\ell| \kappa^{\ell-1} \langle H \rangle^{(\ell)} \right) - n[m(1-\kappa) + 1] \langle H \rangle_{\mathbf{0}}.$$

Appendix B: Symmetries of the QAOA SK cost function landscape

In this appendix, we show that a certain set of transformations of the parameters of the QAOA SK cost function landscape generate a symmetry group of the cost function landscape. The numerical data in the SM suggests this list set of generators extensive. The symmetries are not broken under a general class of noise models which we call the spatio-temporally correlated Pauli noise channels.

The class of Pauli channels contains all channels of the form

$$\Lambda(\rho) = \sum_a P_a \rho P_a^\dagger,$$

with $\{P_a\}_a$ tensor products of the Pauli operators $\{\mathbb{1}, X, Y, Z\}$. Note that Pauli channels can be given the following interpretation: with probability p_a , the Pauli word P_a acts on ρ . We generalize this to circuits with multiple layers and insert Pauli words according to a correlated probability distribution.

Definition B.1 (Spatio-temporally correlated Pauli channels). Let $U = U_g \dots U_1$ be a noiseless quantum circuit consisting of the unitaries $\{U_i\}_i$. The spatio-temporally correlated Pauli error channels are of the form

$$\Lambda(\rho) = \sum_a p_a \tilde{U}_a \rho \tilde{U}_a^\dagger,$$

with

$$\tilde{U}_a = \prod_{i=1}^g (P_{a_i} U_i)$$

the circuit realization in case of noise realization a .

Note that the fluctuator models of the main text are spatio-temporally correlated Pauli error channels if the error operation V is a Pauli operator. Also note that if a set of transformations generate a symmetry group of cost function landscape, also the inverses of the transformations, and any composition of transformations, form symmetries of the cost function landscape.

Lemma B.1. Any n -qubit QAOA SK cost function landscape $\tilde{C}(\beta, \gamma)$, obtained using any number of SWAP-gates, and obtained while the ansatz circuit was acted upon by any spatio-temporally correlated Pauli error channel, is invariant under the group generated by the following transformations.

1. Translation of any γ_k by 2π ,
2. Translation of any β_k by 1π .
3. Negation of any β_k (i.e. $\beta_k \mapsto -\beta_k$) and simultaneous translation of γ_k and γ_{k+1} by π . (For the last β -parameter, that is, the edge case $k = r$, only $\gamma_k = \gamma_r$ needs to be translated by π .)

4. Simultaneous negation of all parameters.

Proof. Let us first assume the QAOA circuit is implemented noiselessly. The first generator follows directly from the periodicity of $RZZ(\gamma)$ with period 2π . For the second generator, note that $RX(\beta \pm \pi) \hat{=} X RX(\beta)$, with $\hat{=}$ denoting equality up to a global phase. Thus, sending $\beta_k \mapsto \beta_k \pm \pi$ has the same effect on the ansatz state as adding a layer of X -gates just before the layer of RX gates of cycle k . Now, note that the layer of X gates commutes with all RZZ gates, any SWAP gates, and all layer of RX gates at all cycles of the ansatz circuit. Thus, we may commute the layer of X -gates all the way to the beginning of the circuit, and act with it on the initial state, resulting in $X^{\otimes n} |+\rangle^{\otimes n} = |+\rangle^{\otimes n}$. Thus, the ansatz state $|\beta\gamma\rangle$ is invariant under $\beta_k \mapsto \beta_k \pm \pi$ for any k , and consequently $\tilde{C}(\gamma, \beta)$ is invariant under these transformations.

For the third generator, note that $RZZ[\pm'(\gamma \pm'' \pi)] \hat{=} Z \otimes Z RZZ[\pm'(\gamma \pm'' \pi)]$. (The signs \pm' and \pm'' are independent.) Thus, sending $\gamma_k \mapsto \gamma_k \pm' \pi$ has the same effect as adding $Z \otimes Z$ to the circuit just after every RZZ -gate in the Hamiltonian stage of cycle k . Note $Z_i Z_j$ commutes with $RZZ_{kl}(x)$ for all x, i, j, k, l , and that any SWAP-gate can be seen as permuting qubit indices, not changing the number of times a qubit is acted on by an RZZ -gate. We may now commute all excess Z -gates that arose from the shift $\gamma_k \mapsto \gamma_k \pm'' \pi$ to just before the layer of RX gates of cycle k . At this layer, every qubit is now acted on by an uneven number of Z -gates, which is equal to the situation where every qubit is acted on by a single Z -gate. We can do the same for cycle $k+1$ of the ansatz circuit, sending $\gamma_k \mapsto \gamma_k \pm'' \pi$, but now moving the resulting Z -gates to just before the layer of RX gates of cycle k . Using $Z_i RX_i(\beta_k) Z_i = RX_i(-\beta_k)$ on all qubits proves the standard case of generator 3. For the edge case $k=r$, sending $\gamma_r \mapsto \gamma_r \pm'' \pi$ results in a layer of Z -gates just before the last layer of RX gates. Commuting this layer through the last layer of RX gates sends β_r to $-\beta_r$. Noting that the layer of Z -gates commutes through (any term of) H , and thus that $\langle \beta, \gamma | Z^{\otimes n} H Z^{\otimes n} | \beta, \gamma \rangle = \langle \beta, \gamma | H | \beta, \gamma \rangle = \tilde{C}(\beta, \gamma)$, completes the proof of generator 3 (in the noiseless case).

The 4th generator follows because (in the computational basis) (i) any gate in the ansatz is generated by a real Hamiltonian, (ii) the Hamiltonian used in QAOA is real, and (iii), the initial state is real. Both $U(\theta) = RX(\theta)$ and $U(\theta) = RZZ(\theta)$ are generated by real Hamiltonians [i.e. statement (i) holds]. Thus, for both operators, $U^T(\theta) = U^\dagger(-\theta)$ and, likewise, $U^{\dagger T}(\theta) = U(-\theta)$. From (ii) and (iii), it follows that $H^T = H$ and $(|+\rangle^n)^T = \langle +|^n$. Let the sequence of gates in the ansatz

be given by $\Pi_{i=g}^1 U_i(\theta_i)$, with g the number of gates in the ansatz, and note that trivially $x = x^T$ for x a real number. Then,

$$\begin{aligned} \tilde{C}(\beta, \gamma) &= (\langle +|^n [\Pi_{i=1}^g U_i^\dagger(\theta_i)] H [\Pi_{i=g}^1 U_i(\theta_i)] |+\rangle^n)^T \\ &= \langle +|^n [\Pi_{i=1}^g U_i^\dagger(-\theta_i)] H [\Pi_{i=g}^1 U_i(-\theta_i)] |+\rangle^n \\ &= \tilde{C}(-\beta, -\gamma). \end{aligned}$$

This completes the proof of Lemma B.1 in the noiseless case.

In case the ansatz circuit is acted upon by a spatio-temporally correlated Pauli error channel,

$$\begin{aligned} \tilde{C}(\beta, \gamma) &= \sum_a p_a \langle +|^{\otimes n} \tilde{U}_a^\dagger(\beta, \gamma) H \tilde{U}_a(\beta, \gamma) |+\rangle^{\otimes n} \\ &:= \sum_a p_a \tilde{C}_a(\beta, \gamma). \end{aligned}$$

So, to show that $\tilde{C}(\beta, \gamma)$ is invariant under the transformations generated by 1–4, it suffices to show that $\tilde{C}_a(\beta, \gamma)$, the cost function in case of realization a , is invariant under those transformations for all noise realizations a .

Transformation 1 trivially leaves $\tilde{C}_a(\beta, \gamma)$ invariant under a spatio-temporally correlated Pauli error channel. To show that the transformations 2 and 3 leave $\tilde{C}_a(\beta, \gamma)$ invariant under the same type of channel, consider $U_a(\beta, \gamma)$, the circuit in case of noise realization a . Note that any Pauli operator either commutes or anti-commutes with both the layer of X -gates arising from any the parameter shift $RX(\beta \pm \pi) \hat{=} X RX(\beta)$, and any $Z \otimes Z$ operators originating from $RZZ[\pm'(\gamma \pm'' \pi)] \hat{=} Z \otimes Z RZZ[\pm'(\gamma \pm'' \pi)]$. Hence, we can use the noiseless proofs of 2–3 to show $C_a(\beta, \gamma)$ is invariant for all a if we make the additional observation that any overall factors of -1 , arising from anti-commutativity, have no effect on the expectation value $C_a(\beta, \gamma)$.

To show generator 4 leaves $\tilde{C}_a(\beta, \gamma)$ invariant, note $RZZ_{ij} = RZZ_{ji}$, and that $RZZ(\theta) P_i = P_i RZZ_{ij}(-\theta)$, if $P_i = X_i$ or $P_i = Y_i$, and $RZZ_{ij}(\theta) P_i = P_i RZZ_{ij}(\theta)$ if $P_i = Z$. Likewise, $RX(\theta) P = P RX(-\theta)$ if $P = Y$ or $P = Z$, and $RX(\theta) P = P RX(\theta)$ if $P = X$. Commuting all Pauli operators arising from an error realization to the beginning of the circuit, we obtain $\tilde{U}_a(\beta, \gamma) = U_0(\tilde{\beta}, \tilde{\gamma}) P$, with P some tensor product of Pauli operators, \tilde{U}_0 the noiseless circuit realization, and where $\tilde{\beta}, \tilde{\gamma}$ can be determined explicitly using the aforementioned commutation relations. Thus, $U_a(\beta, \gamma) |+\rangle^{\otimes n} = U_0(\tilde{\beta}, \tilde{\gamma}) |\psi\rangle$, with $|\psi\rangle$ a state with real entries. Thus, conditions *i-iii* used in the noiseless proof of generator 4 are satisfied, and therefore $C_a(\beta, \gamma) = C_a(-\beta, -\gamma)$. \square